Int. J. Solids Structures, 1968, Vol. 4, pp. 43 to 60. Pergamon Press. Printed in Great Britain

A FINITE ELEMENT APPROXIMATION FOR THE ANALYSIS OF THIN SHELLS

RAY W. CLOUGH and C. PHILIP JOHNSON

University of California, Berkeley

Abstract—An approximate numerical analysis procedure is presented which is capable of solving thin shells of arbitrary shape, boundary conditions and loading. The shell is idealized as an assemblage of triangular finite elements representing both membrane and flexural stiffness properties, and the solution is carried out by digital computer. Five examples are presented which demonstrate the versatility of the procedure in treating different shell configurations, as well as the accuracy of the results which may be obtained.

INTRODUCTION

THE widespread use of thin shell structures has created a need for a systematic method of analysis which can adequately account for arbitrary geometric form and boundary conditions, as well as arbitrary general types of loading. Classical mathematical solutions have serious limitations in practice because unusual geometries or boundary conditions lead to prohibitive complexities in their differential equations of equilibrium. Various numerical procedures have been formulated to deal with special geometric shapes, such as shallow translational shells for example, but generally these are severely limited in applicability.

The purpose of this paper is to describe a numerical shell analysis procedure which avoids all such limitations. It is as effective in treating arbitrary free form surfaces as it is with the simplest geometric shapes. Any types or distributions of applied loadings may be considered, no limitations are imposed with regard to the boundary conditions, and the shell properties may vary in any specified fashion from one portion of the surface to another.

The solution presented herein is based on the finite element method, a technique which was first applied to the solution of plane stress problems [1] and which subsequently has been extended to analysis of axi-symmetric solids and plate bending problems [2], and to axi-symmetric shells [3]. The procedure also has been used previously in thin shell analysis, to a limited extent [4, 5].

The basic concept of the finite element procedure is the idealization of the actual continuum as an assemblage of discrete structural elements. In the present shell analysis program, the arbitrary shell surface is approximated by a system of triangular flat plate elements, the corner (or nodal) points of which lie on the mid-surface of the actual smoothly curved shell. The solution requires first the evaluation of the stiffness properties of the individual elements; the stiffness properties of the complete assemblage are then derived by superposition of the element stiffness. Finally, the analysis of the shell is accomplished by simultaneous solution of the discrete nodal point equilibrium equations for the nodal displacements.

It is important to note that the finite element idealization of the shell introduces two forms of approximation into the analysis. First, the set of flat triangular plate "facets"

provides only an approximation to the smoothly curved surface of the actual shell. Thus the shell which is analyzed differs slightly from the actual shell. Second, the stiffness properties of the individual elements are derived on the basis of an assumed set of displacement patterns within the elements; thus constraints are imposed on the manner of deformation of the shell. However, the errors associated with both types of approximation tend to diminish with reduced mesh sizes in the finite element idealization, and the results of the examples presented in this paper demonstrate that excellent solutions can be obtained with reasonable mesh refinements.

THE FINITE ELEMENT IDEALIZATION

A finite element idealization of a typical shell surface is shown in Fig. 1. The actual smoothly curved surface is approximated by the assemblage of flat, triangular plate elements. The proportions of the elements are arbitrary; they are defined by the coordinates of the nodal points which lie in the mid-surface of the actual shell.

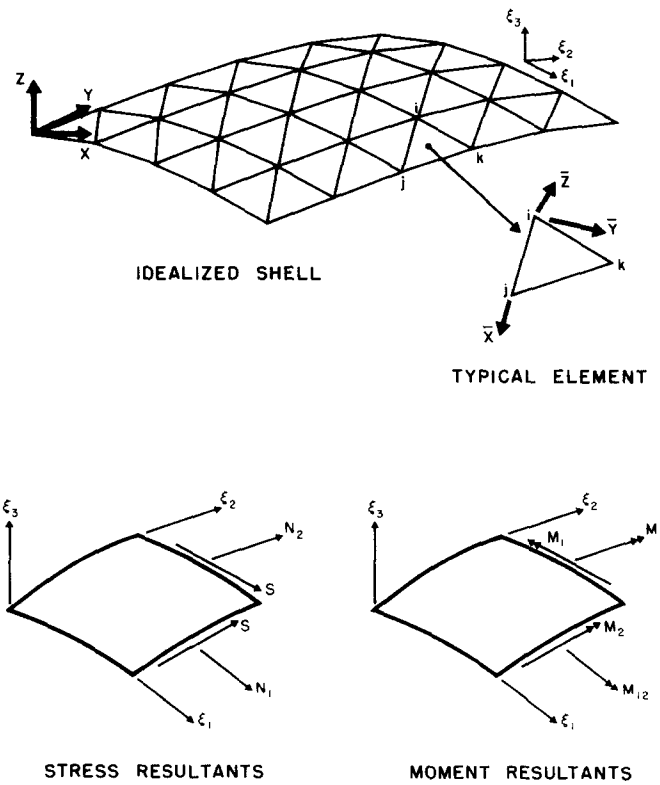

FIG. 1. Typical finite element idealization.

The most critical step in the finite elements analysis is the evaluation of the stiffness properties of the individual elements. It is assumed that the elements are interconnected only at their corner points, thus the element stiffness represents the forces at these nodal

points resulting from unit displacement of the nodal points. Two types of element stiffness are considered in the shell analysis: membrane stiffness which relates forces and displacements in the plane of the elements, and plate bending stiffness which takes account of displacements and rotations out of the element plane. Because the element is a flat plate, there is no coupling between these types of element stiffness properties; therefore it was possible to use a standard plane stress element to represent the membrane stiffness of the shell [1], and a standard plate bending element to represent its flexural stiffness [6].

Because the use of both of these finite element systems has been described in previous publications, it will not be necessary to discuss their derivation in detail here. However, a few comments may be useful to the reader who is unfamiliar with the finite element method. As was mentioned above, the analysis of the element stiffness properties is based upon a set of assumed displacement functions which define the deformations permitted within the element. In general, if these displacement functions are selected so that they maintain full compatibility of displacements along the edges of adjacent elements, and if they also contain the rigid body displacements and uniform stress states of the element, then the solutions provided by the finite element idealization will converge toward the true solution as the element mesh is refined.

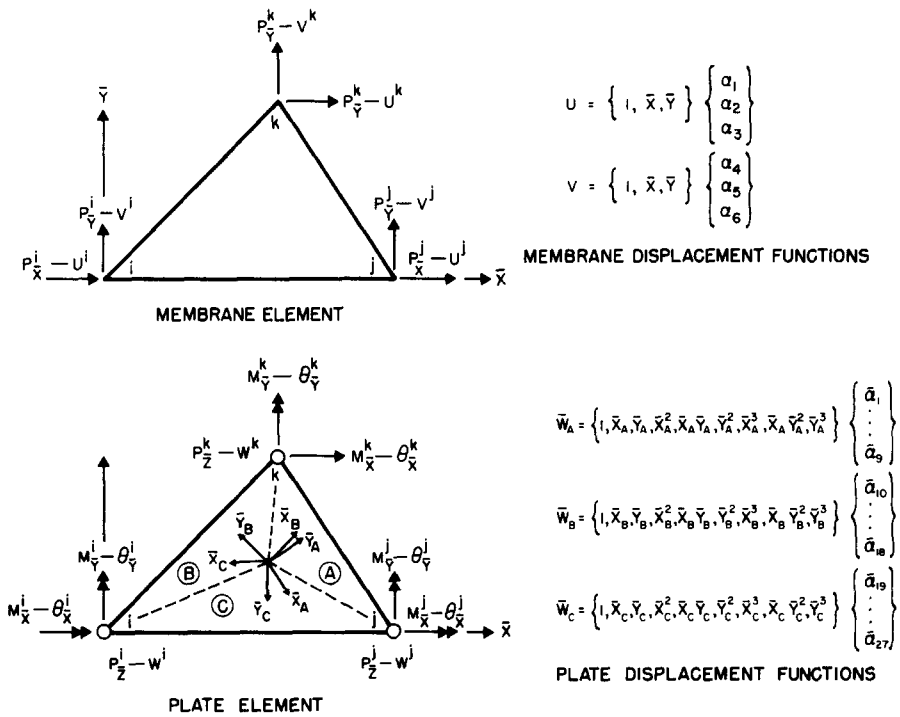

FIG. 2. Membrane and plate element.

Typical membrane and plate bending elements are shown in Fig. 2, together with the displacement functions assumed in evaluating their stiffness matrices. The membrane element has two degrees of freedom at each nodal point, and the displacements are assumed

to vary linearly between the nodal points [1]. It is evident that such displacement patterns will provide full compatibility for a system of elements lying in a plane. The plate bending element has three degrees of freedom at each nodal point (two rotations and the normal translation), thus a total of 9 independent displacement functions should be specified. In this case, however, in order to develop displacement functions which maintain full compatibility along the edges, it was necessary to divide the plate into three subelements and assume nine displacement functions in each subelement. These twenty-seven displacement shapes were then reduced to nine independent patterns by applying internal compatibility constrains between the subelements [6]. In this idealization the transverse displacements, w, vary as cubic functions within the element.

The analysis of the element stiffness properties from any given set of displacement functions may be carried out by a standard sequence of matrix operations [2]. The result for a membrane element may be expressed as:

$$\begin{Bmatrix} \bar{\boldsymbol{\beta}}_m^i \\ \bar{\boldsymbol{\beta}}_m^j \\ \bar{\boldsymbol{\beta}}_m^k \end{Bmatrix} = [\bar{K}_m] \begin{Bmatrix} \bar{\mathbf{V}}_m^i \\ \bar{\mathbf{V}}_m^j \\ \bar{\mathbf{V}}_m^k \end{Bmatrix} \tag{1}$$

where for a typical node "i" (see Fig. 2):

$$\bar{\boldsymbol{\beta}}_m^i = \begin{Bmatrix} P_{\bar{x}}^i \\ P_{\bar{y}}^i \end{Bmatrix} \quad \text{and} \quad \bar{\mathbf{V}}_m^i = \begin{Bmatrix} U^i \\ V^i \end{Bmatrix}. \tag{2}$$

Similarly, the stiffness of a plate bending element is:

$$\begin{Bmatrix} \bar{\boldsymbol{\beta}}_P^i \\ \bar{\boldsymbol{\beta}}_P^j \\ \bar{\boldsymbol{\beta}}_P^k \end{Bmatrix} = [\bar{K}_P] \begin{Bmatrix} \bar{\mathbf{V}}_P^i \\ \bar{\mathbf{V}}_P^j \\ \bar{\mathbf{V}}_P^k \end{Bmatrix} \tag{3}$$

where for node "i" (Fig. 2)

$$\boldsymbol{\beta}_P^i = \begin{Bmatrix} P_{\bar{z}}^i \\ M_{\bar{x}}^i \\ M_{\bar{y}}^i \end{Bmatrix} \quad \text{and} \quad \bar{\mathbf{V}}_P^i = \begin{Bmatrix} W^i \\ \theta_{\bar{x}}^i \\ \theta_{\bar{y}}^i \end{Bmatrix}. \tag{4}$$

The complete membrane plus flexural stiffness of the element, therefore, may be expressed symbolically as:

$$\begin{Bmatrix} \bar{\boldsymbol{\beta}}_m \\ \bar{\boldsymbol{\beta}}_P \end{Bmatrix} = \begin{bmatrix} \bar{K}_m & 0 \\ 0 & \bar{K}_P \end{bmatrix} \begin{Bmatrix} \bar{\mathbf{V}}_m \\ \bar{\mathbf{V}}_P \end{Bmatrix} \tag{5}$$

wherein the element is assumed to have a total of 15 degrees of freedom, five at each nodal point.

It should be noted that the displacement functions assumed in defining these element stiffness properties will not, in general, satisfy displacement compatibility conditions between adjacent elements of a shell idealization. The displacements were chosen to maintain compatibility of both membrane and flexural displacements in finite element idealizations of any plane system. However, when the elements do not lie in the same plane,

the plate bending deformations produce membrane type discontinuities of a form which cannot be corrected by the membrane displacements. Fortunately, this type of discrepancy diminishes with decreasing mesh size (i.e. as the elements tend to be more nearly co-planar) and appears to have no significant adverse effect on the solution.

FORMING THE ELEMENT ASSEMBLAGE

The stiffness matrix of the complete element assemblage may be determined most conveniently by the direct stiffness procedure. To accomplish this, it is necessary first to transform the stiffness matrices for the individual elements to a common coordinate system, called herein the base coordinates; then the stiffness of the assemblage is obtained merely by adding together the appropriate components of the element stiffness matrices.

In the analysis of shell structures, it is convenient to employ two different types of coordinate systems in establishing the base coordinates: a fixed set of Cartesian coordinates (x, y, z) which are called the global coordinates, and surface coordinates (ξ_1, ξ_2, ξ_3) in which ξ_3 is taken normal to the shell surface at every point. In addition, the individual element properties are defined initially in terms of the element coordinate system $(\bar{x}, \bar{y}, \bar{z})$ specified for each element. All of these coordinate systems are shown in Fig. 1.

The transformations from element and surface coordinates to global coordinates may be expressed as:

$$\begin{Bmatrix} Q_x \\ Q_y \\ Q_z \end{Bmatrix} = [\overline{\mathbf{T}}] \begin{Bmatrix} P_{\bar{x}} \\ P_{\bar{y}} \\ P_{\bar{z}} \end{Bmatrix} \quad \text{and} \quad \begin{Bmatrix} Q_x \\ Q_y \\ Q_z \end{Bmatrix} = [\mathbf{T}_\xi] \begin{Bmatrix} P_{\xi_1} \\ P_{\xi_2} \\ P_{\xi_3} \end{Bmatrix} \tag{6}$$

or

$$\mathbf{Q} = \overline{\mathbf{T}}\,\overline{\mathbf{P}} \quad \text{and} \quad \mathbf{Q} = \mathbf{T}_\xi \mathbf{P}_\xi \tag{7}$$

where $\mathbf{Q}$, $\overline{\mathbf{P}}$, $\mathbf{P}_\xi$ represent similar force quantities expressed in global coordinates, element coordinates, and surface coordinates respectively; and $\overline{\mathbf{T}}$ and $\mathbf{T}_\xi$ represent the usual direction cosines. By equating these two expressions (equation 7), the transformation from element coordinates to surface coordinates may be obtained:

$$\mathbf{P}_\xi = \mathbf{T}_\xi^T \overline{\mathbf{T}}\overline{\mathbf{P}} \equiv \overline{\mathbf{T}}_\xi \overline{\mathbf{P}}. \tag{8}$$

The matrices $(\overline{\mathbf{T}}, \mathbf{T}_\xi, \overline{\mathbf{T}}_\xi)$ define all the necessary transformations for force and displacement quantities, provided no constraints are placed on these quantities. However, in the stiffness matrix defined for each element only two rotational degrees of freedom are considered at each node. Accordingly, only two rotational degrees of freedom per nodal point were included in the base system describing the assembled structure. These are referred to the surface coordinates ξ_1 and ξ_2. The third rotation quantity, about ξ_3, was neglected because for a good mesh representation each triangle associated with a given node will lie close to the tangent plane of the node. It was assumed that rotation about the normal to the tangent plane would be negligible in the actual shell and results from numerous examples have verified this assumption. The moment transformation of the two

rotational degrees of freedom which are considered is:

$$\begin{Bmatrix} M_{\xi_1} \\ M_{\xi_2} \end{Bmatrix} = [\mathbf{T}_c] \begin{Bmatrix} M_{\bar{x}} \\ M_{\bar{y}} \end{Bmatrix} \tag{9}$$

where $\mathbf{T}_c$ is the upper left 2×2 block of $\overline{\mathbf{T}}_\xi$.

The transformation of the element stiffness to base coordinates for a typical element is accomplished by rearranging equation (5) so that the five degrees of freedom at each corner are grouped together:

$$\begin{Bmatrix} \bar{\boldsymbol{\beta}}^i \\ \bar{\boldsymbol{\beta}}^j \\ \bar{\boldsymbol{\beta}}^k \end{Bmatrix} = [\bar{\mathbf{K}}] \begin{Bmatrix} \mathbf{V}^i \\ \mathbf{V}^j \\ \mathbf{V}^k \end{Bmatrix} \tag{10}$$

where typical forces and displacements for node "i" are (see Fig. 2):

$$\bar{\boldsymbol{\beta}}^i = \begin{Bmatrix} M_{\bar{x}}^i \\ M_{\bar{y}}^i \\ P_{\bar{x}}^i \\ P_{\bar{y}}^i \\ P_{\bar{z}}^i \end{Bmatrix} \quad \text{and} \quad \bar{\mathbf{V}}^i = \begin{Bmatrix} \theta_{\bar{x}}^i \\ \theta_{\bar{y}}^i \\ U^i \\ V^i \\ W^i \end{Bmatrix} \tag{11}$$

If global coordinates are used for the three linear displacements, then the appropriate transformation matrix is:

$$\mathbf{T} \equiv \begin{bmatrix} \mathbf{T}_c^i & & & & & \\ & \overline{\mathbf{T}} & & & & \\ & & \mathbf{T}_c^j & & & \\ & & & \overline{\mathbf{T}} & & \\ & & & & \mathbf{T}_c^k & \\ & & & & & \overline{\mathbf{T}} \end{bmatrix} \tag{12}$$

where $\mathbf{T}_c^i$, $\mathbf{T}_c^j$, $\mathbf{T}_c^k$ are transformations of the type of equation (9), defined at points i, j, and k respectively. Then the transformed element stiffness, $\mathbf{k}$, expressed in the base coordinates is given by:

$$\mathbf{k} = \mathbf{T}\bar{\mathbf{K}}\mathbf{T}^T \tag{13}$$

where $\bar{\mathbf{K}}$ represents the element stiffness expressed in its element coordinates. It is to be emphasized that the base coordinates defined here are global coordinates for the translational degrees of freedom, but are surface coordinates for the rotational degrees of freedom, and that only two rotational degrees of freedom are included (the membrane rotation about the normal being set equal to zero).

In the finite element analysis of any shell, the stiffness of each element in the idealization is transformed to the common base coordinate system as shown in equation (13). The

contribution of each element may then be added directly into the (base coordinate) stiffness matrix **K** of the complete structure, as indicated in Fig. 3.

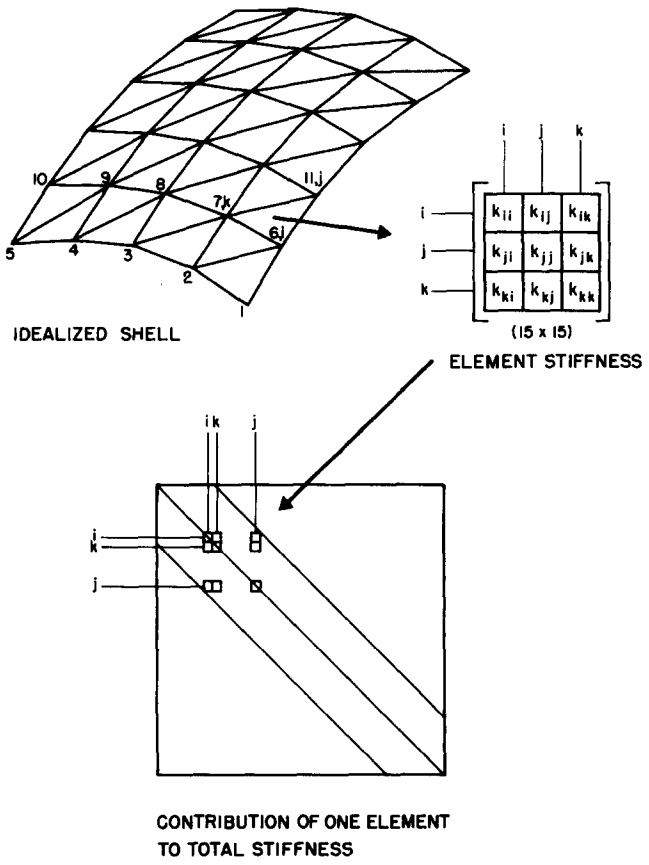

FIG. 3. Direct stiffness formulation of the structure stiffness matrix.

SOLUTION OF THE EQUILIBRIUM EQUATIONS

The stiffness matrix **K** of the finite element idealization serves to relate the nodal loads **R** acting on the shell to the resulting nodal displacements **v**:

$$\mathbf{Kv} = \mathbf{R}. \tag{14}$$

In its initial formulation, **K** contains five degrees of freedom for each nodal point in the element assemblage. Before equation (14) may be solved, however, the boundary conditions of the shell must be recognized. This may be accomplished conveniently by striking out the rows and columns of the degrees of freedom associated with the boundary constraints and by replacing the corresponding diagonal term with a non-zero value. The constraints may be applied in arbitrary combinations of the five degrees of freedom considered at each nodal point. No consideration is given to the rotation about the normal.

The load vector **R** in equation (14) represents the values of the force components applied at the nodes of the assembled structure. These may be applied arbitrarily, but they usually include only linear forces. The nodal forces resulting from distributed loads generally are computed from simple tributary area considerations.

The stiffness matrix **K** of equation (14) may be characterized, in general, as (1) symmetric, (2) banded, (3) positive definite, (4) sparsely populated. Algorithms which utilize either iterative methods or direct methods for the solution of equations with these properties are well known. A direct method (triangular decomposition) was used to obtain the results presented herein; therefore, a brief discussion of the above properties related to this procedure is pertinent.

The first three properties are very significant when related to the direct solution of large systems of equations. Symmetry permits a reduction of approximately one half in the number of calculations. The banding property permits one to consider only the coefficients contained within the band width since it is preserved during the solution. The positive definite property insures stability of the solution; hence, the solution may be obtained without pivoting. These properties thus enable one to obtain a direct solution by keeping only a small portion of the stiffness matrix in high speed memory at any time, while sequentially retrieving and storing additional information by means of relatively slow input–output devices such as tapes and disks. The portion of the stiffness matrix required to be in core at any time during the solution determines how large the band width can be. The minimum storage required is $m(m+1)/2$ where m is the half band width, and this requires retrieving and storing information in blocks of m numbers. For a 32K core the maximum half band width permitted is approximately 200. If larger blocks of information are to be used for input–output, then the band width must be reduced.

A typical triangle element mesh (8×12) suitable for analysis of a cylindrical shell, for example, and a schematic diagram of the assembled element stiffness matrix are shown in Fig. 4. Since each node has five degrees of freedom, the total number of unknowns, n, is 585. The half band width, m, is 50. To obtain the half band width the entire array of elements is scanned and the maximum difference between the numbers of any two nodes associated with a particular triangle is recorded. The half band width is then given by one plus this number multiplied by five. The shaded zones in the stiffness matrix indicate the maximum horizontal spread of the non-zero coefficients. It is interesting to note that if this mesh were subdivided to 16×24 subdivisions, each shaded area would retain the same width while the half band width would be increased to 90. Unfortunately, this type of sparseness does not permit a reduction in computational effort. The number of multiplications required to decompose the structure stiffness matrix is approximately $nm^2/2$. The number of additions are also approximately $nm^2/2$. Typical times, in seconds, required for the decomposition and the back substitution for problems which have been run on the IBM 7094 are:

Mesh	m	n	Decomposition	Back substitutions
4×5	30	150	5	3
8×12	50	585	37	18
12×18	70	1235	159	44
16×22	90	1955	340	77

The algorithm used to solve these equations is written in FORTRAN IV, using disk storage for the back substitutions.

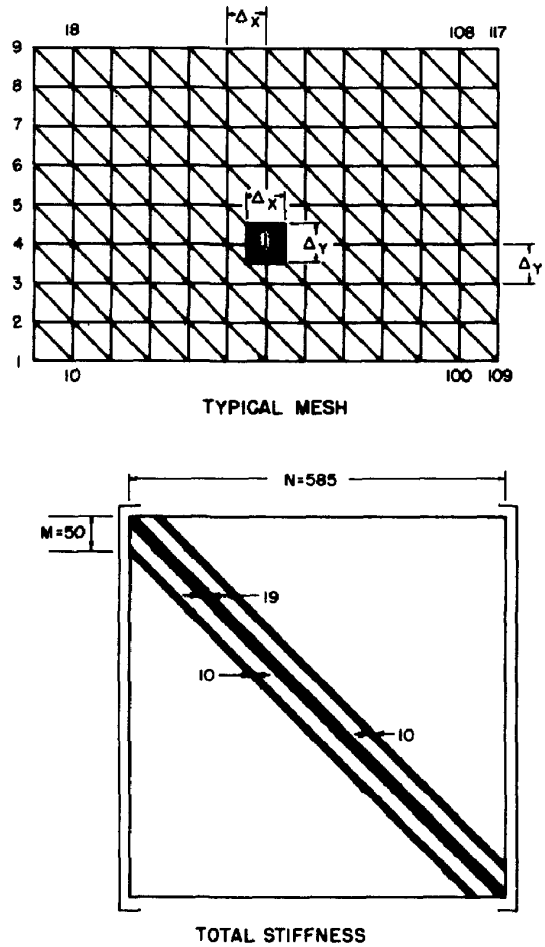

FIG. 4. Banding property of typical stiffness matrix.

The solution of the equilibrium equations yields the displacement components of the nodal points of the finite element system. From these nodal displacements, it is a relatively simple matter to determine the element deformations inasmuch as the element displacements are limited to the assumed patterns. Thus the stresses in each element also may be determined from the nodal displacements, by taking account of the material stress-strain properties. In general, the stresses in adjacent elements will not be found to be continuous. Even if no displacement discontinuities were present it should be evident that the assumed displacement patterns cannot insure local stress equilibrium across the element boundaries (although the gross equilibrium of the system is satisfied by the nodal forces). In the present program a weighted averaging process has been used to determine stress values at the nodal points from the stresses in all the elements surrounding each nodal point.

RESULTS OF ANALYSIS

In order to demonstrate the capability and versatility of this finite element shell analysis procedure, analyses have been made of a wide range of thin shell systems involving many different forms of shell geometry and boundary conditions. Because of space limitations only a few examples of smoothly curved shell surfaces will be discussed here. Results have been obtained in each case for all displacement and stress components, but only selected typical data will be presented. Comparisons with results obtained by other analytical procedures are included for each case.

Spherical dome (Examples 1 and 2)

The first case to be considered is the spherical dome subjected to external pressure loading which is shown in Fig. 5. Because of its axial symmetry, it was possible to treat a single segment of this system in the finite element idealization. A 30° segment of the sphere was considered, and the element nodes were located on parallel arcs at meridional angle intervals of 2·5 degrees—making a total of 14 arcs over the full 35 degree meridional angle.

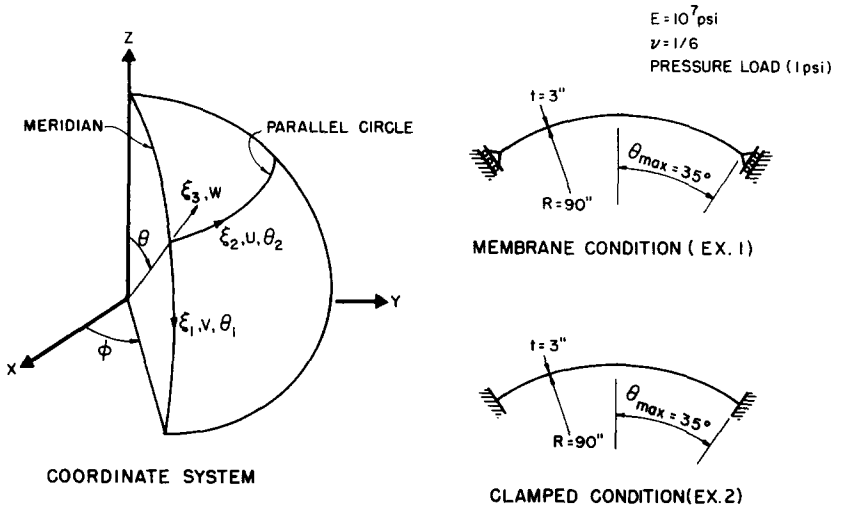

FIG. 5. Axisymmetric spherical dome (Examples 1 and 2).

Two cases were considered for this shell: Example 1 was supported on rollers at the boundary so as to maintain a membrane state of stress, while Example 2 was clamped at the edge. Results of Example 1 agreed almost exactly with the membrane theory—displacements were correct to three significant figures at all nodes and stresses were well within one percent of the theoretical values. The meridional moment and hoop stresses determined for the clamped case (Example 2) are shown in Fig. 6, in comparison with "exact" results for this case, taken from Ref. [7]. The slight deviation of the finite element results which may be noted near the clamped edge could have been reduced by refining the mesh in this region.

Circular cylinder (Example 3)

The second form of shell to be discussed is a circular cylinder, loaded by its own dead weight, supported by diaphragms at the ends, and free along the sides. Because of its

double symmetry only one-quarter of this shell was considered in the analysis, as shown in Fig. 7. The end diaphragm was assumed to be infinitely rigid in its own plane and infinitely flexible out of that plane.

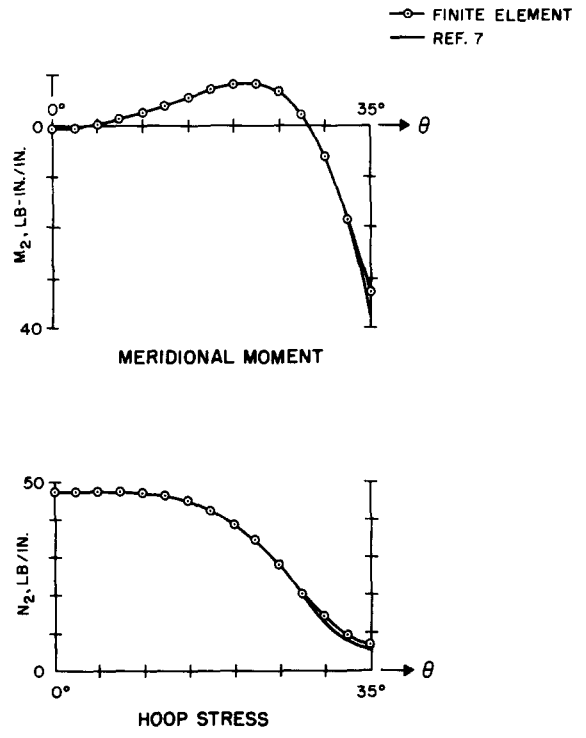

FIG. 6. Sphere with clamped edge (Example 2).

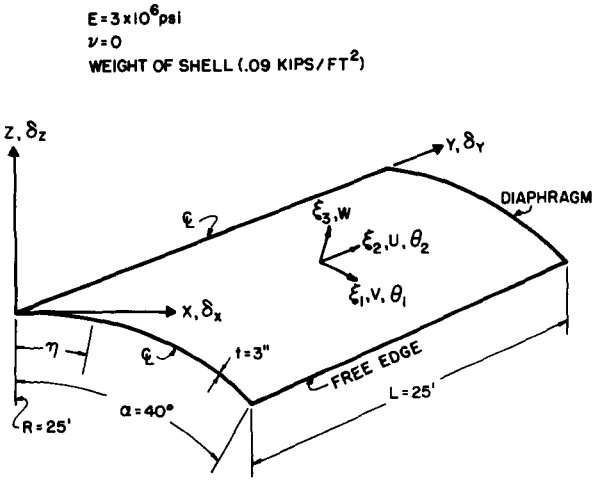

FIG. 7. Circular cylinder (Example 3).

Four different mesh sizes were considered in this analysis in order to demonstrate the convergence of results toward the correct values. Vertical displacements (δ_z) across the mid-section, determined for the four different meshes, are presented in Fig. 8. Also shown is the "exact" result computed by numerical evaluation of the Donnel–Jenkins shell equation [8]. The displacements are seen to have the correct form in each analysis, but the finest mesh was required to provide essential convergence to the true results. The results obtained from the fine mesh analysis for the longitudinal displacements at the end diaphragm

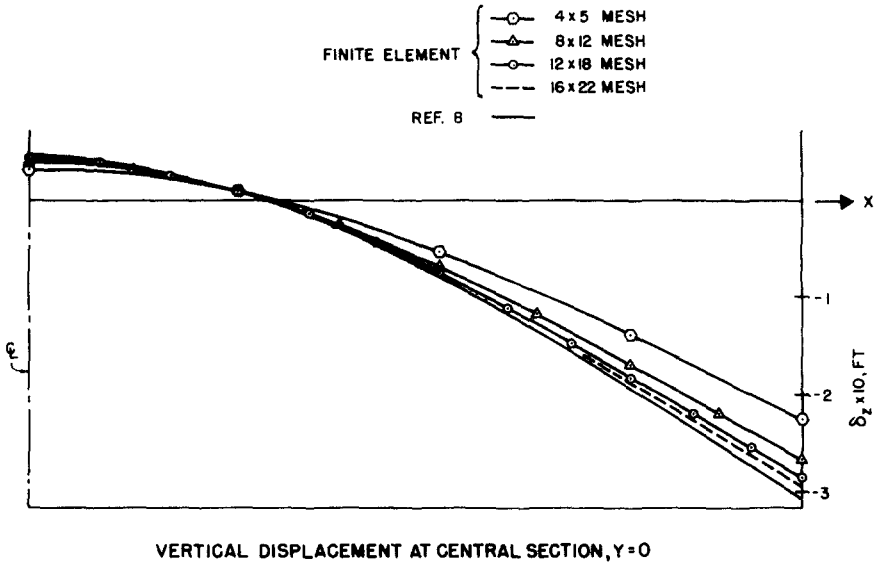

FIG. 8. Circular cylinder (Example 3), vertical displacement at central section, $Y = 0$.

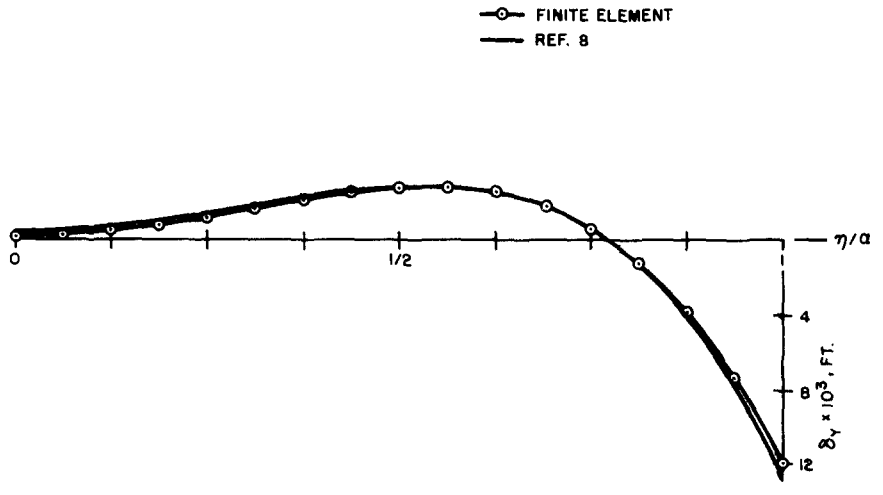

FIG. 9. Circular cylinder (Example 3), longitudinal displacement at diaphragm, $Y = L$.

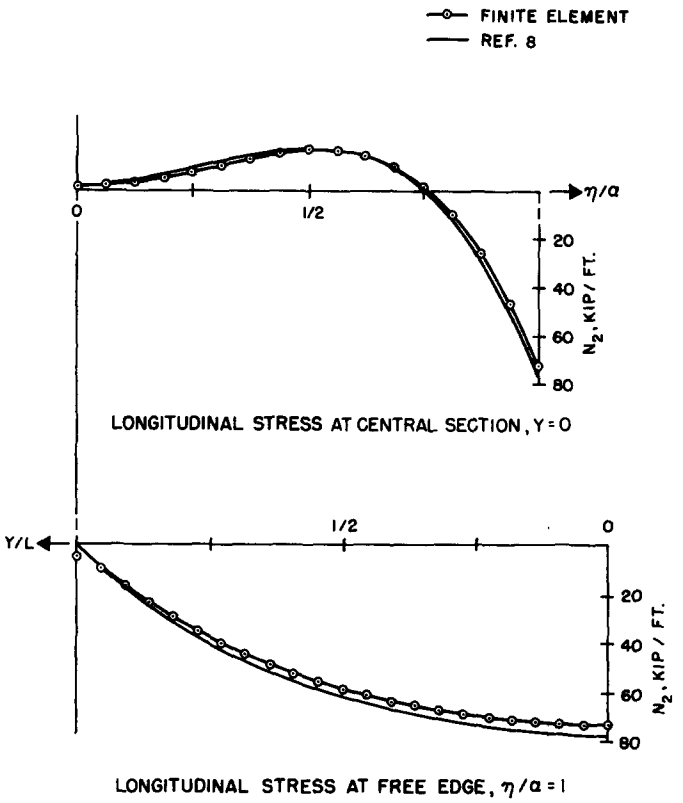

FIG. 10. Circular cylinder (Example 3).

and for two of the stress components are presented in Figs. 9 and 10, respectively. In addition, three components of bending moment are shown in Fig. 11. Agreement with the Donnel–Jenkins shell theory results is seen to be good in all figures, but complete convergence apparently has not yet been achieved.

Translational shells (Example 4)

In this example, three different forms of shells are considered and compared: a parabolic cylinder (PC), an elliptic paraboloid (EP, positive Gaussian curvature), and a hyperbolic paraboloid (HP, negative Gaussian curvature) as shown in Fig. 12. Each shell has the same transverse parabolic profile and is supported at the ends by a diaphragm normal to the shell surface, while the longitudinal edges are free. Loading of each shell is due to its own dead weight.

Certain results of the finite element analyses are presented in Fig. 13 in comparison with the numerical analysis results presented in Ref. [9]. Uniform rectangular mesh layouts (12×18 mesh for the first two shell types, 8×12 mesh for the hyperbolic paraboloid) were used in the analyses with dimensions as shown on the figure. The finite element results for the parabolic cylinder are seen to check well with those given in the reference. The agreement of the longitudinal stresses for the hyperbolic paraboloid also is seen to be excellent,

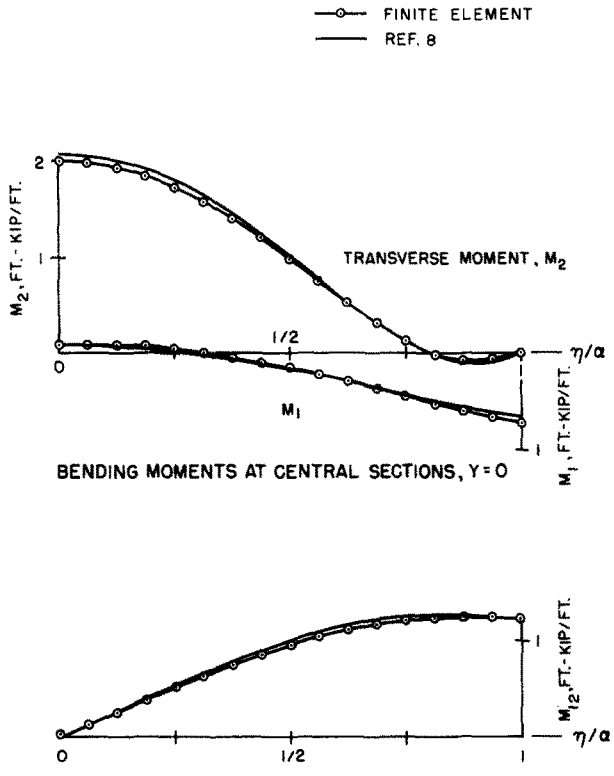

FIG. 11. Circular cylinder (Example 3).

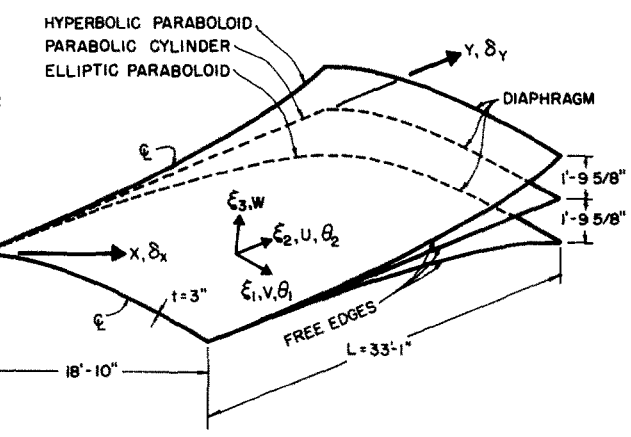

FIG. 12. Translational shells (Example 4).

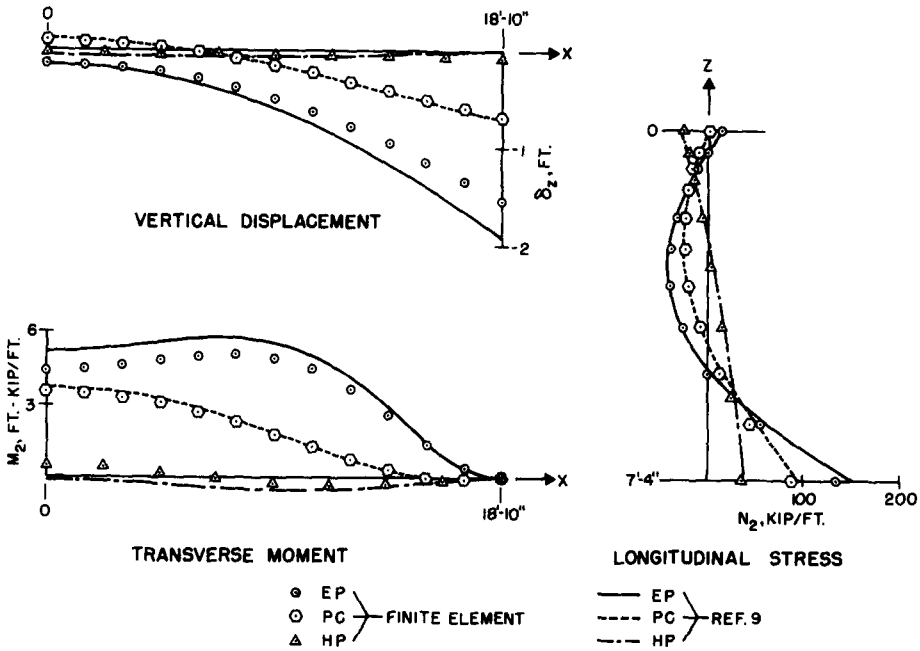

FIG. 13. Translation shells (Example 4), comparison of results at central section $Y = 0$.

although the vertical displacements and transverse moments for this shell show some slight deviations. This discrepancy is not significant, however, inasmuch as the values are so small.

The greatest discrepancies are found in the case of the elliptic paraboloid. Even in this case, the deviations are not severe, and may be explained in part by the fact that a slightly different structure was considered in Ref. [9]. The shallow shell theory used in that analysis required that the longitudinal profile be assumed in the form of a circular arc while the finite element analysis took account of the true parabolic profile.

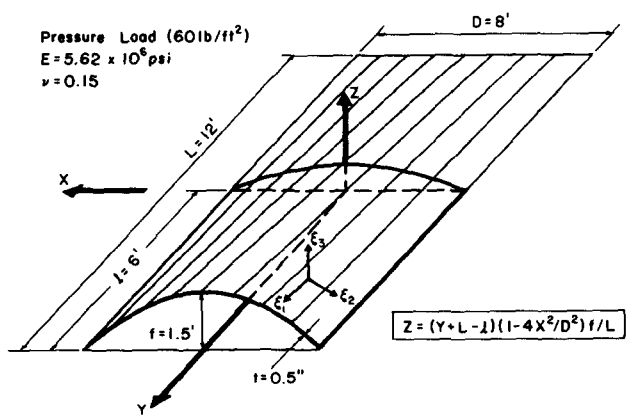

FIG. 14. Conoid (Example 5).

Conoid (Example 5)

The conoidal shell, shown in Fig. 14, is supported on all four sides by diaphragms normal to the shell surface, and is subjected to an external pressure load. Only half the shell was treated in the analysis, due to symmetry, using a uniform 12×18 rectangular mesh (referred to the horizontal plane).

The normal displacement components and transverse moments computed by the finite element procedure are shown in Fig. 15, while two in-plane stress components are shown in Fig. 16. Also shown are some results derived from shallow shell theory which were presented in Ref. [10]. The general form of the two sets of results is in agreement, but significant differences in magnitude are evident. In this case, it is believed that the finite element results are the more reliable because this shell has a significantly greater rise than would be permitted by shallow shell theory.

CONCLUSIONS

The examples presented herein demonstrate the versatility of the finite element procedure in treating shells of arbitrary configuration. Assemblages of triangular elements

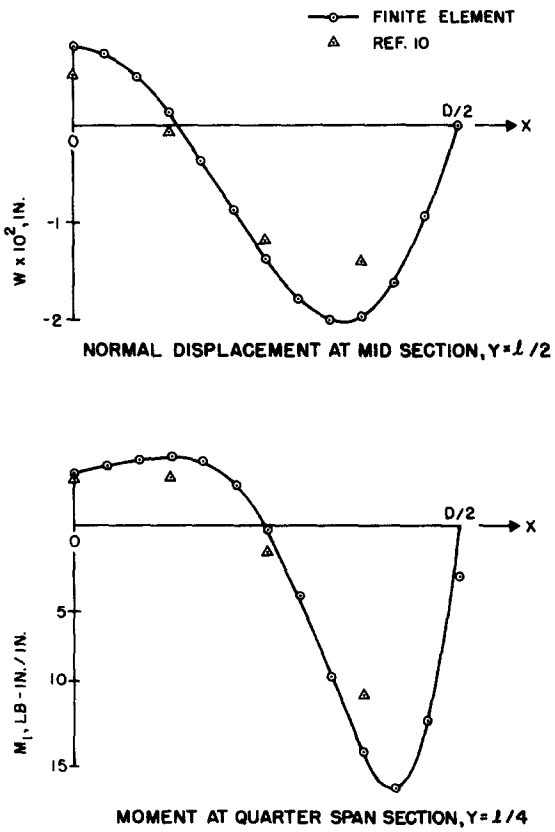

FIG. 15. Conoid (Example 5).

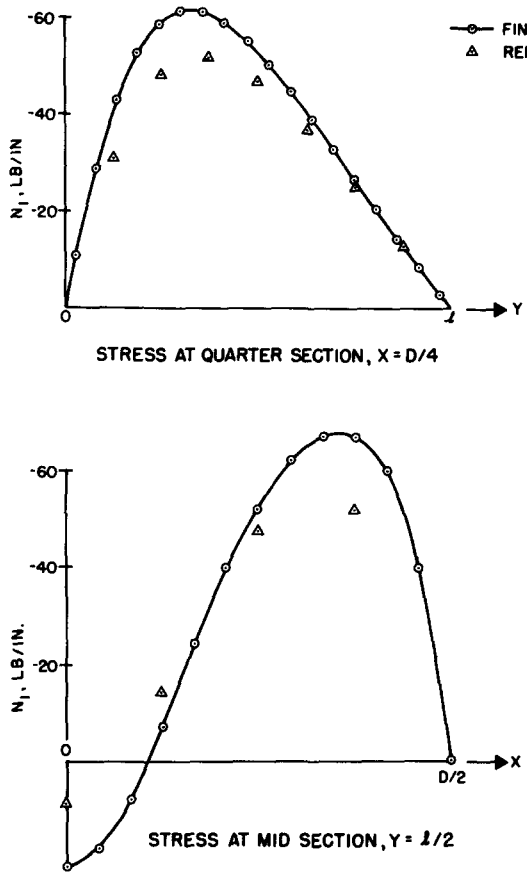

FIG. 16. Conoid (Example 5).

can be established to approximate any surface form, and the mesh size can be varied conveniently so that small elements may be utilized in regions of sharp curvature together with larger elements in flatter portions of the shell. It is important to note that the discrete element idealization also permits the analysis of shells of varying thickness or having variations in any of the material properties. The idealization considered here assumes all properties to be constant within each element, but they may change arbitrarily from element to element. Moreover, it is not difficult to account for orthotropic material properties in the element stiffness analysis, rather than isotropic properties such as were considered in these examples.

The results of the examples considered herein are seen to represent good approximations to the exact solutions derived by other procedures in the cases where such solutions are available, and the analysis of the cylindrical shell demonstrates the convergence of the process as the finite element mesh is refined. Thus it seems reasonable to conclude that equivalent accuracy and convergence properties would be obtained in the analysis of other shell configurations. At present no means is available for evaluating quantitatively the error which may result from the physical approximation of the shell; i.e., the substitution of a system of flat plate "facets" for a smoothly curved surface. On the other hand, the use of

assumed displacement functions in the analysis of the element stiffness properties is merely a special form of Rayleigh–Ritz analysis, and conclusions regarding the convergence of that process are applicable to the finite element procedure if full compatibility can be maintained in the assumed displacement functions.

As a final comment it is worth noting that further developments may be made in the finite element analysis of shells. Work is under way at the present time directed toward the derivation of more refined planar elements which can represent more complex stress distributions within the elements, as well as singly and doubly curved elements which may provide better approximations to the geometry of the given shell.

Acknowledgement—The research program on the development of finite element procedures for the analysis of thin shells, which is reported in part in this paper, was supported by research grant No. GK-75 from the National Science Foundation. This financial assistance is gratefully acknowledged.

REFERENCES

[1] M. J. TURNER, R. W. CLOUGH, H. C. MARTIN and L. J. TOPP, Stiffness and deflection analysis of complex structures. *J. aeronaut. Sci.* **23**, No. 9 (1956).
[2] R. W. CLOUGH, The finite element method in structural mechanics. *Stress Analysis*, edited by O. C. ZIENKIEWICZ, G. S. HOLISTER. Wiley (1965).
[3] P. E. GRAFTON and D. R. STROME, Analysis of axisymmetrical shells by the direct stiffness method. *AIAA Jnl* **1**, 2347 (1963).
[4] R. W. CLOUGH and J. L. TOCHER, Analysis of thin arch dams by the finite element method. *Theory of Arch Dams*, edited by J. R. RYDZEWSKI. Pergamon Press (1964).
[5] O. C. ZIENKIEWICZ and Y. K. CHEUNG, Finite element method of analysis for arch dam shells and comparison with finite difference procedures. *Theory of Arch Dams*, edited by J. R. RYDZEWSKI. Pergamon Press (1964).
[6] R. W. CLOUGH and J. L. TOCHER, Finite element stiffness matrices for the analysis of plate bending. *Proc. Conf. Matrix Methods in Structural Mechanics*, Air Force Institute of Technology, Wright–Patterson Air Force Base, Ohio, October 1965.
[7] S. TIMOSHENKO and S. WOINOWSKY-KRIEGER, *Theory of Plates and Shells*, Engineering Societies Monographs. McGraw-Hill (1959).
[8] A. C. SCORDELIS and K. S. LO, Computer analysis of cylindrical shells. *J. Am. Concr. Inst.* **61**, No. 5 (1964).
[9] A. W. HEDGREN, A numerical and experimental study of translational shell roofs, Ph.D. Dissertation, Princeton University (Oct. 1965).
[10] H. A. HADID, An analytical and experimental investigation into the bending theory of elastic conoidal shells, Ph.D. Dissertation, Univ. of Southampton (March 1964).

(*Received* 16 *January* 1967; *revised* 5 June 1967)

Абстракт—Приводится приближенный численный метод, весьма пригодный для расчета тонких оболочек произвольной формы, произвольных граничных условий и нагрузки. Оболочка идеализируется в виде совокупности конечных трехугольных элементов, обладающх мембранным состоянием а также жесткостью на изгиб. Решение получается используя счетные машины. Приводится пять примеров, которые указуют многосторонность метода расчета при обработке разных очертаний оболочек, как и точность полученых результатов.